

MetaFood CVPR 2024 Challenge on Physically Informed 3D Food Reconstruction: Methods and Results

Workshop and Challenge Organizers

Jiangpeng He¹, Yuhao Chen², Gautham Vinod¹, Talha Ibn Mahmud¹

Fengqing Zhu¹, Edward Delp¹, Alexander Wong², Pengcheng Xi³

¹ Purdue University ² University of Waterloo ³ National Research Council Canada

Challenge Winner Team - First Place

Ahmad AlMughrabi⁴, Umair Haroon⁴, Ricardo Marques⁴, Petia Radeva⁴

⁴ Universitat de Barcelona

Challenge Winner Team - Second Place

Jiadong Tang⁵, Dianyi Yang⁵, Yu Gao⁵, Zhaoxiang Liang⁵

⁵ Beijing Institute of Technology

Challenge Winner Team - Best 3D Mesh Reconstruction

Yawei Jueluo⁶, Chengyu Shi⁷, Pengyu Wang⁸

⁶ Baidu Inc. ⁷ XPeng Motors ⁸ Beijing University of Posts and Telecommunications

Abstract

The increasing interest in computer vision applications for nutrition and dietary monitoring has led to the development of advanced 3D reconstruction techniques for food items. However, the scarcity of high-quality data and limited collaboration between industry and academia have constrained progress in this field. Building on recent advancements in 3D reconstruction, we host the MetaFood Workshop and its challenge for Physically Informed 3D Food Reconstruction. This challenge focuses on reconstructing volume-accurate 3D models of food items from 2D images, using a visible checkerboard as a size reference. Participants were tasked with reconstructing 3D models for 20 selected food items of varying difficulty levels: easy, medium, and hard. The easy level provides 200 images, the medium level provides 30 images, and the hard level provides only 1 image for reconstruction. In total, 16 teams submitted results in the final testing phase. The solutions developed in this challenge achieved promising results in 3D food reconstruction, with significant poten-

tial for improving portion estimation for dietary assessment and nutritional monitoring. More details about this workshop challenge and access to the dataset can be found at <https://sites.google.com/view/cvpr-metafood-2024>.

1. Introduction

The intersection of computer vision and culinary arts has opened new frontiers in dietary monitoring and nutritional analysis. The CVPR 2024 MetaFood Workshop Challenge represents a significant step in this direction, addressing the growing need for accurate, scalable methods of food portion estimation and nutritional intake tracking. These technologies are crucial to promote healthy eating habits and managing diet-related health conditions.

By focusing on reconstructing accurate 3D models of food items from both multi-view and single-view inputs, this challenge aims to bridge the gap between existing methods and real-world requirements. The challenge encourages the development of innovative techniques that can handle

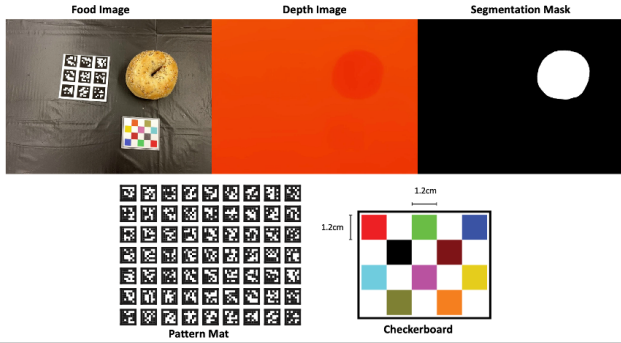


Figure 1. Sample challenge data for “everything bagel”.

the complexities of food shapes, textures, and lighting conditions, while also addressing the practical constraints of real-world dietary assessment scenarios. By bringing together researchers and practitioners in computer vision, machine learning, and nutrition science, this challenge seeks to catalyze advancements in 3D food reconstruction that could significantly improve the accuracy and applicability of food portion estimation in various contexts, from personal health monitoring to large-scale nutritional studies.

Traditional diet assessment methods [44], such as 24-Hour Recall or Food Frequency Questionnaire (FFQ), often rely on manual input, which can be inaccurate and cumbersome. Furthermore, the absence of 3D information in 2D RGB food images presents significant challenges for regression-based methods [10, 35] that estimate food portions directly from eating occasion images. By advancing 3D reconstruction techniques for food items, we aim to offer more precise and intuitive tools for nutritional assessment. This technology has the potential to improve the sharing of food experiences and significantly impact fields such as nutrition science and public health.

The challenge tasked participants with reconstructing 3D models of 20 selected food items from 2D images, simulating a scenario where a cellphone with a depth camera is used for food logging and nutritional monitoring. It was structured into three difficulty levels. The easy level food object provided approximately 200 frames uniformly sampled from video, the medium level offered about 30 images, and the hard level presented participants with a single monocular top-view image. This structure was designed to test the robustness and versatility of the proposed solutions across various real-world scenarios. A sample hard food object is shown in Figure 1. The key features of the challenge include the use of a visible checkerboard as a physical reference, as well as the availability of the depth image for each video frame, ensuring that the reconstructed 3D models maintain accurate real-world scaling for portion size estimation.

This challenge not only pushes the boundaries of 3D re-

construction technology, but also paves the way for more accurate, robust, and user-friendly applications in the real world, such as image-based dietary assessment. The solutions developed here have the potential to significantly impact how we monitor and understand our nutritional intake, contributing to broader goals in health and wellness. As we continue to advance in this field, we anticipate seeing innovative applications that could revolutionize personal health management, nutritional research, and the food industry at large. The structure of this technical report is as follows. In Section 2, we review existing related work for food portion size estimation. In Section 3, we introduce the dataset used for this challenge and the detailed evaluation pipelines. Finally, we summarize the methodology and experimental results for the three winner teams (*VoLETA*, *ININ-VIAUN*, *FoodRiddle*) in Section 4, Section 5, and Section 6, respectively.

2. Related Work

Food portion estimation is an important component of image-based dietary assessment [11, 36] with the goal of estimating the volume, energy or macronutrients directly from the input eating occasion images. Compared to the widely studied food recognition task [9, 12, 14, 24–27], food portion estimation presents a unique challenge due to the absence of 3D information and physical references, which are essential for accurately inferring the real-world size of food portions. Specifically, accurately estimating portion sizes requires an understanding of the volume and density of the food, aspects that cannot be easily determined from a two-dimensional image, which highlights the need for advanced methodologies and technologies to address this issue. Existing food portion estimation methods can be categorized into four main groups [23].

Stereo-Based Approach. These methods rely on multiple frames to reconstruct the 3D structure of the food. In [28], food volume is estimated using multi-view stereo reconstruction based on epipolar geometry. Similarly, [29] performs two-view dense reconstruction. Simultaneous Localization and Mapping (SLAM) is utilized in [8] for continuous and real-time food volume estimation. The primary limitation of these methods is the requirement for multiple images, which is impractical for real-world deployment.

Model-Based Approach. Predefined shapes and templates are leveraged to estimate the target volume. For instance, [49] assigns certain templates to foods from a library and applies transformations based on physical references to estimate the size and location of the food. A similar template matching approach is used in [16] to estimate food volume from a single image. However, these methods cannot accommodate variations in food shapes that deviate from predefined templates. The most recent work [46] leveraged the 3D food mesh as the template to align both camera pose and

object pose for portion size estimation.

Depth Camera-Based Approach. The depth camera is utilized to produce a depth map that captures the distance from the camera to the food in the image. In [22, 37], the depth map is used to form a voxel representation of the image, which is then used to estimate the food volume. The main limitation is the requirement for high-quality depth maps and additional post-processing needed for consumer depth sensors.

Deep Learning Approach. Neural network-based methods leverage the abundance of image data to train complex networks for food portion estimation. Regression networks are used in [35, 45] to estimate the energy value of food from a single image input and from an “Energy Distribution Map,” which maps the input image to the energy distribution of the foods in the image. In [43], regression networks trained on input images and depth maps produce energy, mass, and macronutrient information for the food(s) in the image. Deep learning-based methods require large amounts of data for training and are generally not explainable. Their performance often degrades when the input test image differs significantly from the training data.

Although these approaches have made significant strides in food portion estimation, they all face limitations that hinder their widespread adoption and accuracy in real world scenarios. Stereo-based methods are impractical for single-image input, model-based approaches struggle with diverse food shapes, depth camera-based methods require specialized hardware, and deep learning approaches lack explainability and struggle with out-of-distribution samples. To address these challenges, 3D reconstruction offers a promising solution by providing comprehensive spatial information, adapting to various food shapes, potentially working with single images, offering visually interpretable results, and enabling a standardized approach to food portion estimation. These advantages motivated the organization of the 3D Food Reconstruction challenge, with the aim of overcoming existing limitations and developing more accurate, user-friendly, and widely applicable food portion estimation techniques that can significantly impact nutritional assessment and dietary monitoring.

3. Datasets and Evaluation Pipeline

3.1. Dataset Description

The MetaFood Challenge dataset comprises 20 carefully selected food items from MetaFood3D dataset¹, each scanned with a 3D scanner and accompanied by corresponding video captures. To ensure accurate size representation in the reconstructed 3D models, each item was captured alongside a checkerboard and pattern mat, serving as physical references for scaling. The challenge is structured into three

¹MetaFood3D - the dataset can be accessed at this link.

difficulty levels, determined by the number of 2D images available for reconstruction:

- Easy: Approximately 200 images sampled from video
- Medium: 30 images
- Hard: A single monocular top-view image

Table 1 provides detailed information about the food items in the dataset.

Object Index	Food Item	Difficulty Level	Number of Frames
1	Strawberry	Easy	199
2	Cinnamon bun	Easy	200
3	Pork rib	Easy	200
4	Corn	Easy	200
5	French toast	Easy	200
6	Sandwich	Easy	200
7	Burger	Easy	200
8	Cake	Easy	200
9	Blueberry muffin	Medium	30
10	Banana	Medium	30
11	Salmon	Medium	30
12	Steak	Medium	30
13	Burrito	Medium	30
14	Hotdog	Medium	30
15	Chicken nugget	Medium	30
16	Everything bagel	Hard	1
17	Croissant	Hard	1
18	Shrimp	Hard	1
19	Waffle	Hard	1
20	Pizza	Hard	1

Table 1. MetaFood Challenge Data Details

3.2. Evaluation Pipeline

The evaluation process consists of two phases, focusing on the precision of the reconstructed 3D models in terms of their shape (3D structure) and portion size (volume).

3.2.1 Phase-I: Volume Accuracy

In the first phase, we employ Mean Absolute Percentage Error (MAPE) as the metric to assess the accuracy of portion size. The MAPE is calculated as follows:

$$MAPE = \frac{1}{n} \sum_{i=1}^n \left| \frac{A_i - F_i}{A_i} \right| \times 100\% \quad (1)$$

where A_i is the groundtruth volume (in unit of ml) of the i -th food object obtained from the scanned 3D food mesh, and F_i is the volume obtained from the reconstructed 3D mesh.

3.2.2 Phase-II: Shape Accuracy

The top-ranking teams from Phase-I are invited to submit complete 3D mesh files for each food item. This phase involves several steps to ensure accuracy and fairness:

- **Model Verification:** We verify the submitted models against the final Phase-I submissions to ensure consistency. Additionally, we conduct visual inspections to prevent rule violations, such as submitting primitive objects (e.g., spheres) instead of detailed reconstructions.
- **Model Alignment:** We will provide participants with the ground truth 3D models, along with the script used to compute the final Chamfer distance. Participants are required to align their models with the ground truth and prepare a transform matrix for each submitted object. The final Chamfer distance score will be computed using these submitted models and transformation matrices.
- **Chamfer Distance Calculation:** The shape accuracy is evaluated using the Chamfer distance metric. Given two point sets X and Y , the Chamfer distance is defined as in the following.

$$d_{CD}(X, Y) = \frac{1}{|X|} \sum_{x \in X} \min_{y \in Y} \|x - y\|_2 + \frac{1}{|Y|} \sum_{y \in Y} \min_{x \in X} \|x - y\|_2 \quad (2)$$

This metric provides a comprehensive measure of the similarity between the reconstructed 3D models and the ground truth. The final ranking will be determined by combining the scores from both Phase-I (volume accuracy) and Phase-II (shape accuracy). Note that after the Phase-I evaluation, we observed some quality issues with the provided data for object 12 (steak) and object 15 (chicken nugget). To ensure the quality and fairness of the competition, we have decided to exclude these two items from the final overall evaluation process.

4. First Place Team - VoIETA

4.1. Methodology

The team’s study utilizes multi-view reconstruction to create intricate food meshes and calculate precise food volumes. The source code is available at <https://github.com/GCVCG/VoIETA-MetaFood>.

4.1.1 Overview

The team’s approach combines computer vision and deep learning techniques to estimate food volume from RGBD images and masks accurately. Keyframe selection ensures data quality, aided by perceptual hashing and blur detection. Camera pose estimation and object segmentation lay the groundwork for neural surface reconstruction, producing detailed meshes for volume estimation. Refinement steps enhance accuracy, including isolated piece removal and scaling factor adjustment. The team’s approach offers a comprehensive solution for precise food volume assessment with potential applications in nutrition analysis.

4.1.2 The Team’s Proposal: VoIETA

The team begins their approach by acquiring input data, specifically RGBD images and corresponding food object masks. These RGBD images, denoted as $\mathcal{I}^D = \{I_i^D\}_{i=1}^n$, where n is the total number of frames, provide the necessary depth information alongside the RGB images. The food object masks, denoted as $\{M_j^i\}_{i=1}^n$, aid in identifying the regions of interest within these images.

Next, the team proceeds with keyframe selection. From the set $\{I_i^D\}_{i=1}^n$, keyframes $\{I_j^K\}_{j=1}^k \subseteq \{I_i^D\}_{i=1}^n$ are selected. The team implements a method to detect and remove duplicates [15] and blurry images [5] to ensure high-quality frames. This involves applying the Gaussian blurring kernel followed by the fast Fourier transform method. Near-Image Similarity [15] employs a perceptual hashing and hamming distance thresholding to detect similar images and keep overlapping. The duplicates and blurry images are excluded from the selection process to maintain data integrity and accuracy, as shown in Fig. 2(a).

Using the selected keyframes $\{I_j^K\}_{j=1}^k$, the team estimates the camera poses through PixSfM [18] (i.e., extracting features using SuperPoint [7], matching them using SuperGlue [32], and refining them). The outputs are the set of camera poses $\{C_j\}_{j=1}^k$, which are crucial for spatial understanding of the scene.

In parallel, the team utilizes the SAM [17] for reference object segmentation. SAM segments the reference object with a user-provided segmentation prompt (i.e., user click), producing a reference object mask M^R for each keyframe. This mask is a foundation for tracking the reference object across all frames. The team then applies the XMem++ [3] method for memory tracking, which extends the reference object mask M^R to all frames, resulting in a comprehensive set of reference object masks $\{M_i^R\}_{i=1}^n$. This ensures consistency in reference object identification throughout the dataset.

To create RGBA images, the team combines the RGB images, reference object masks $\{M_i^R\}_{i=1}^n$, and food object masks $\{M_i^F\}_{i=1}^n$. This step, denoted as $\{I_i^R\}_{i=1}^n$, integrates the various data sources into a unified format suitable for further processing, as shown in Fig. 2(b).

The team converts the RGBA images $\{I_i^R\}_{i=1}^n$ and camera poses $\{C_j\}_{j=1}^k$ into meaningful metadata and modeled data D_m . This transformation facilitates the accurate reconstruction of the scene.

The modeled data D_m is then input into NeuS2 [47] for mesh reconstruction. NeuS2 generates colorful meshes $\{R_f, R_r\}$ for the reference and food objects, providing detailed 3D representations of the scene components. The team applies the “Remove Isolated Pieces” technique to refine the reconstructed meshes. Given that the scenes contain only one food item, the team sets the diameter threshold to 5% of the mesh size. This method deletes isolated con-

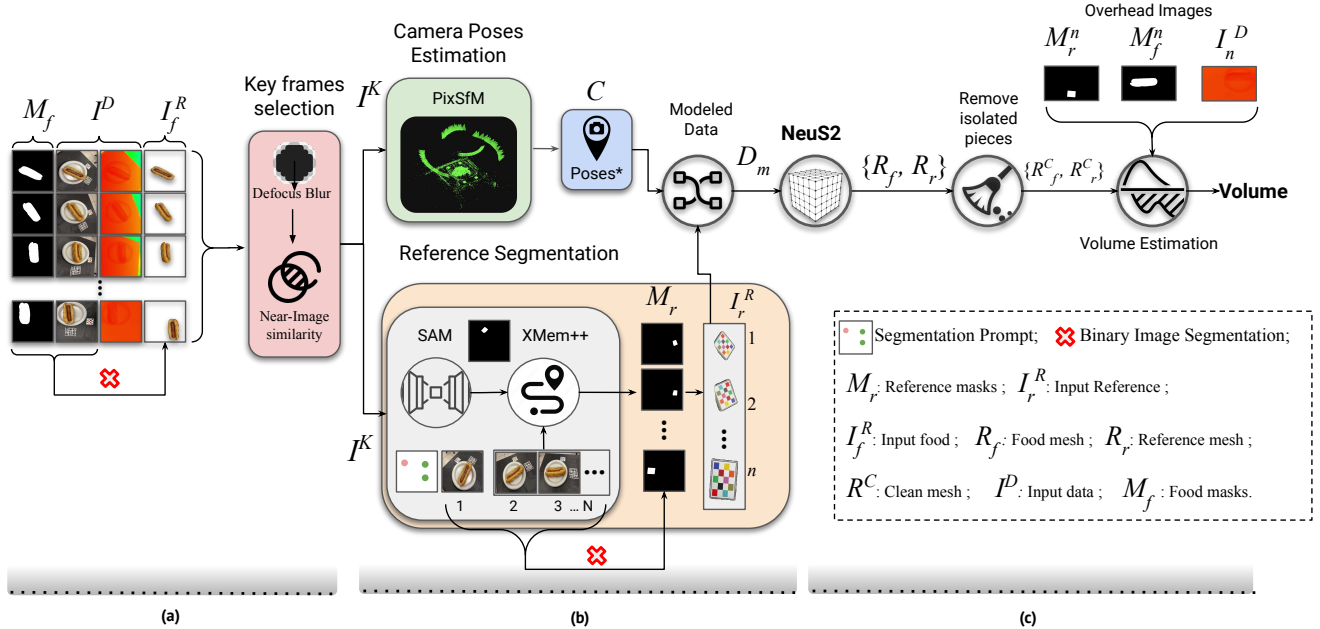


Figure 2. The team’s few-shot approach for estimating food volume in (a) a few shots involves taking (\mathcal{I}^D) and food object masks as input. The team starts by selecting keyframes based on the RGB images, removing blurry and highly overlapped images resulting (\mathcal{I}^K). Then, (b) the team uses PixSfM to estimate camera poses (C). Simultaneously, the team segments the reference object using SAM with a segmentation prompt provided by a user. The team then uses the XMem++ method for memory-tracking to produce reference object masks for all frames, using the reference object mask and RGB images. After that, the team applies a binary image segmentation method to RGB images (\mathcal{I}^K), reference object masks (M_r), and food object masks (M_f), resulting in RGBA images (\mathcal{I}_r^R). In contrast, the team transforms the RGBA images and poses to generate meaningful metadata and create modeled data (D_m). Next, (c) the team inputs the modeled data into NeuS2 to reconstruct colorful meshes for reference (R_r) and food objects (R_f). To ensure accuracy, the team uses “Remove Isolated Pieces” with diameter thresholding to clean up the mesh and remove small isolated pieces that do not belong to the reference or food mesh resulting ($\{R_f^C, R_r^C\}$). Finally, the team manually identifies the scaling factor using the reference mesh via MeshLab (S). The team fine-tunes the scaling factor using depth information and the food masks and then applies the fine-tuned scaling factor (S_f) to the cleaned food mesh to generate a scaled food mesh (R_f^F) in meter unit.

nected components whose diameter is less than or equal to this 5% threshold, resulting in a cleaned mesh $\{R_f^C, R_r^C\}$. This step ensures that only significant and relevant parts of the mesh are retained.

The team manually identifies an initial scaling factor S using the reference mesh via MeshLab [4] for scaling factor identification. This factor is then fine-tuned S_f using depth information and food and reference masks, ensuring accurate scaling relative to real-world dimensions. Finally, the fine-tuned scaling factor S_f is applied to the cleaned food mesh R_f^C , producing the final scaled food mesh R_f^F . This step culminates in an accurately scaled 3D representation of the food object, enabling precise volume estimation, as shown in Fig. 2(c).

4.1.3 Detecting the scaling factor

Generally, 3D reconstruction methods generate unitless meshes (i.e., no physical scale) by default. To overcome this limitation, the team manually identifies the scaling fac-

tor by measuring the distance for each block for the reference object mesh, as shown in Fig. 3b. Next, the team takes the average of all blocks lengths l_{avg} , while the actual real-world length (as shown in Fig. 3a) is constant $l_{real} = 0.012$ in meter. Furthermore, the team applies the scaling factor $S = l_{real}/l_{avg}$ on the clean food mesh R_f^C , producing the final scaled food mesh R_f^F in meter.

The team leverages depth information alongside food and reference object masks to validate the scaling factors. The team’s method for assessing food size entails utilizing overhead RGB images for each scene. Initially, the team determines the pixel-per-unit (PPU) ratio (in meters) using the reference object. Subsequently, the team extracts the food width (f_w) and length (f_l) employing a food object mask. To ascertain the food height (f_h), the team follows a two-step process. Firstly, the team conducts binary image segmentation using the overhead depth and reference images, yielding a segmented depth image for the reference object. The team then calculates the average depth utilizing

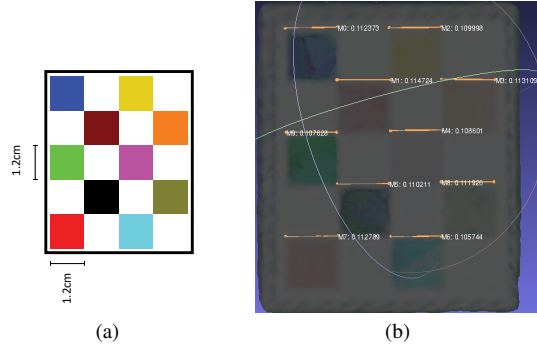


Figure 3. The team manually measures the scaling factor using MeshLab’s Measuring tool. The team measures multiple blocks in the reference object mesh; then, the team takes the average of blocks lengths l_{avg} .

the segmented reference object depth (d_r). Similarly, employing binary image segmentation with an overhead food object mask and depth image, the team computes the average depth for the segmented food depth image (d_f). Finally, the estimated food height f_h is computed as the absolute difference between d_r and d_f . Furthermore, to assess the accuracy of the scaling factor S , the team computes the food bounding box volume ($(f_w \times f_l \times f_h) \times PPU$). The team evaluates if the scaling factor S generates a food volume close to this potential volume, resulting in S_{fine} . Table 2 shows the scaling factors, PPU, 2D Reference object dimensions, 3D food object dimensions, and potential volume.

For one-shot 3D reconstruction, the team leverages One-2-3-45 [20] for reconstructing a 3D from a single RGBA view input after applying binary image segmentation on both food RGB and mask. Next, the team removes isolated pieces from the generated mesh. After that, the team reuses the scaling factor S , which is closer to the potential volume of the clean mesh, as shown in Fig. 4.

4.2. Experimental Results

4.2.1 Implementation settings

The team ran the experiments using two GPUs, GeForce GTX 1080 Ti/12G and RTX 3060/6G. The team set the hamming distance as 12 for the near image similarity. For Gaussian kernel radius, the team set the even numbers in the range [0...30] for detecting blurry images. The team set the diameter as 5% for removing isolated pieces. The number of iteration of NeuS2 is 15000, mesh resolution is 512×512 , the unit cube “aabb_scale” is 1, “scale”: 0.15, and “offset”: [0.5, 0.5, 0.5] for each food scene.

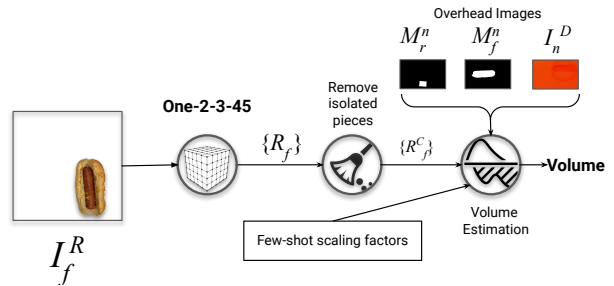


Figure 4. The team’s one-shot food volume estimation approach. The team begins with a food-segmented image (I_f^R), and then uses the One-2-3-45 model to generate a mesh (R_f). Next, the team cleans up the isolated pieces that are less than 5% of the (R_f) size, resulting in a cleaned food mesh R_f^C . Furthermore, the team chooses a scaling factor based on the depth information S_f . Finally, the team applies the chosen scaling factor on R_f^C to have a scaled mesh (R_f^E) where the team extracts the volume.

4.2.2 VoLETA Results

The team extensively validated their approach on the challenge dataset as described in Section 3 and compared their results with ground truth meshes using MAPE and Chamfer distance metrics. More Briefly, the team leverages their approach for each food scene separately. A one-shot food volume estimation approach is applied if the number of keyframes k equals 1. Otherwise, a few-shot food volume estimation is applied. Notably, Fig. 6 shows that the team’s keyframe selection process chooses 34.8% of total frames for the rest of the pipeline, where it shows the minimum frames with the highest information.

After finding the keyframes, PixSfM [18] estimates the poses and point cloud (see Fig. 7).

After generating the scaled meshes, the team calculates the volumes and Chamfer distance with and without transformation metrics. The team registered their meshes and ground truth meshes to obtain the transformation metrics using ICP [30] (see Fig. 8).

Table 3 presents the quantitative comparisons of the team’s volumes and Chamfer distance with and without the estimated transformation metrics from ICP.

For overall method performance, Table 4 shows the MAPE and Chamfer distance with and without transformation metrics.

Additionally, Fig. 5 shows the qualitative results on the one and few-shot 3D reconstruction from the challenge dataset. The figures show that the team’s model excels in texture details, artifact correction, missing data handling, and color adjustment across different scene parts.

Limitations. Despite the promising results demonstrated by the team’s method, several limitations need to be ad-

Level	Id	Label	S_f	PPU	$R_w \times R_l$	$(f_w \times f_l \times f_h)$	Volume (cm^3)
Easy	1	strawberry_2	0.08955223881	0.01786	320 360	238 257 2.353	45.91
	2	cinnamon_bun_1	0.1043478261	0.02347	236 274	363 419 2.353	197.07
	3	pork_rib_2	0.1043478261	0.02381	246 270	435 778 1.176	225.79
	4	corn_2	0.08823529412	0.01897	291 339	262 976 2.353	216.45
	5	french_toast_2	0.1034482759	0.02202	266 292	530 581 2.53	377.66
	6	sandwich_2	0.1276595745	0.02426	230 265	294 431 2.353	175.52
	7	burger_1	0.1043478261	0.02435	208 264	378 400 2.353	211.03
	8	cake_1	0.1276595745	0.02143	256 300	298 310 4.706	199.69
Medium	9	blueberry_muffin	0.08759124088	0.01801	291 357	441 443 2.353	149.12
	10	banana_2	0.08759124088	0.01705	315 377	446 857 1.176	130.80
	11	salmon_1	0.1043478261	0.02390	242 269	201 303 1.176	40.94
	13	burrito_1	0.1034482759	0.02372	244 271	251 917 2.353	304.87
	14	frankfurt_sandwich_2	0.1034482759	0.02115	266 304	400 1022 2.353	430.29
Hard	16	everything_bagel	0.08759124088	0.01747	306 368	458 484 1.176	79.61
	17	croissant_2	0.1276595745	0.01751	319 367	395 695 2.176	183.39
	18	shrimp_2	0.08759124088	0.02021	249 318	186 195 0.987	14.64
	19	waffle_2	0.01034482759	0.01902	294 338	465 537 0.8	72.29
	20	pizza	0.01034482759	0.01913	292 336	442 651 1.176	123.97

Table 2. A list of information that extracted using the RGBD and masks, where the team presents the scene Id, the scaling factor S_{fine} , Pixel-Per-Unit (in cm), 2D reference object dimensions ($R_w \times R_l$), 3D food object dimensions ($f_w \times f_l \times f_h$) in pixels, and the potential volume (in cm^3). The rows in red are excluded meshes.

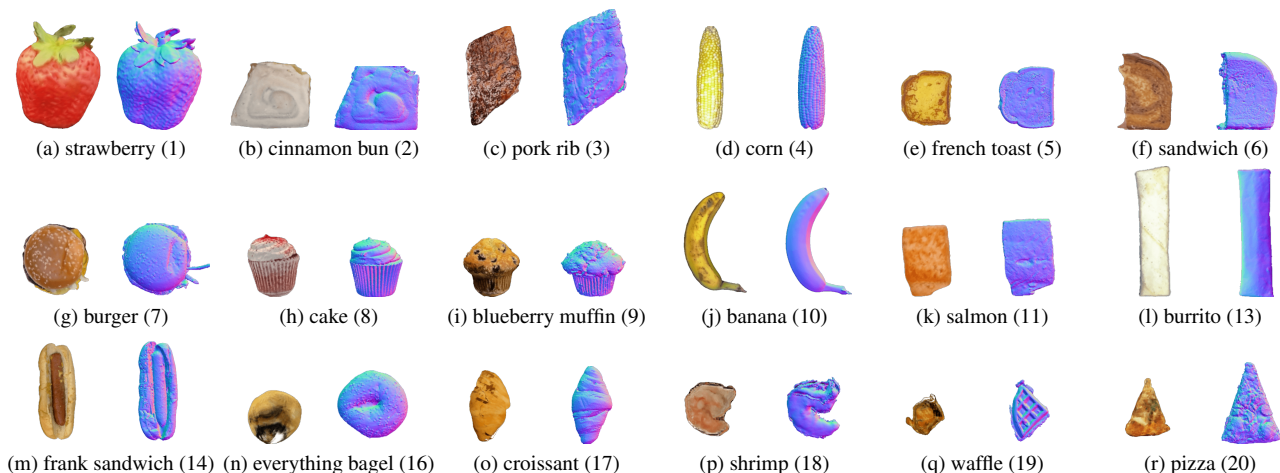


Figure 5. Comparisons to the team’s results and ground truth using the challenge dataset. Each scene shows the team’s reconstruction (left) and ground truth (right).

dressed in future work:

- **Manual processes:** The current pipeline includes manual steps, such as providing a segmentation prompt and identifying scaling factors. These steps should be automated to enhance efficiency and reduce human intervention. This limitation arises from the necessity of using a reference object to compensate for missing data sources, such as Inertial Measurement Unit (IMU) data.
- **Input requirements:** The team’s method requires extensive input information, including food masks and depth data. Streamlining the necessary inputs would simplify the process and potentially increase its applicability in

varied settings.

- **Complex backgrounds and objects:** The team has not tested their method in environments with complex backgrounds or on highly intricate food objects. Applying their approach to datasets with more complex food items, such as the Nutrition5k [43] dataset, would be challenging and could help identify corner cases that need to be addressed.
- **Capturing complexities:** The method has not been evaluated under different capturing complexities, such as varying distances between the camera and the food object, different camera speeds, and other scenarios as de-

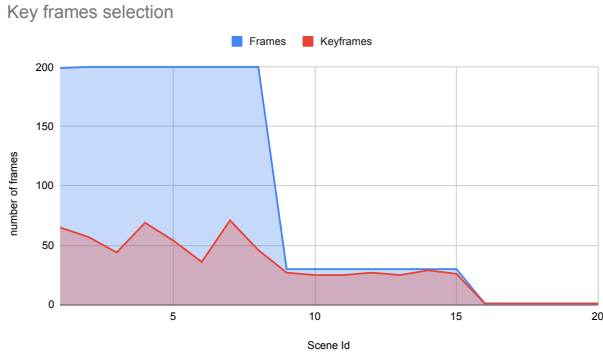


Figure 6. A quantitative results to the number of frames before and after the keyframe selection phase. The team’s approach is only using 34.8% of the data.

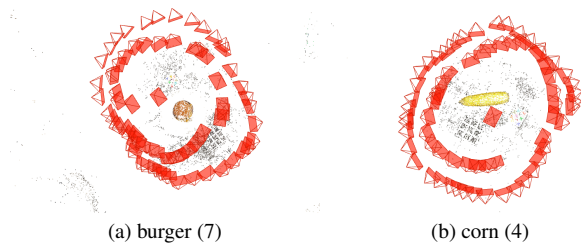


Figure 7. PixSfm results after applying keyframes selection. PixSfm excels in estimating and refining camera poses by providing a rich point cloud using Superpoint feature extractors.

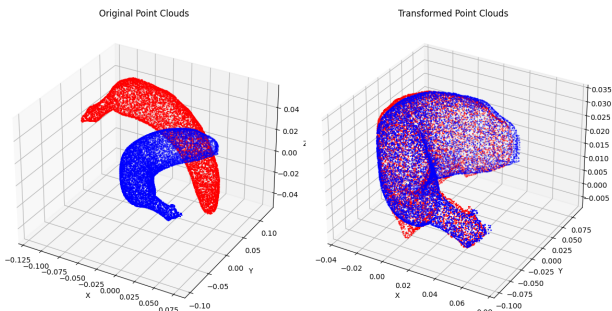


Figure 8. Performed ICP mesh registration between the team’s generated and ground truth meshes for banana_2 scene. Unregistered meshes are on the left, while registered meshes are on the right. The team’s Point cloud is red, and the ground truth is blue.

fined in the Fruits and Vegetables [39] dataset. These factors could significantly impact the performance and robustness of the team’s method.

- **Pipeline complexity:** For one-shot neural rendering, the team currently uses the One-2-3-45 [20] method. However, they aim to use only the 2D diffusion model, Zero123 [21], in their pipeline to reduce complexity and improve the efficiency of their approach.

L	Id	Team’s Vol.	GT Vol.	Ch. w/ t.m	Ch. w/o t.m
E	1	40.06	38.53	1.63	85.40
	2	216.9	280.36	7.12	111.47
	3	278.86	249.67	13.69	172.88
	4	279.02	295.13	2.03	61.30
	5	395.76	392.58	13.67	102.14
	6	205.17	218.44	6.68	150.78
	7	372.93	368.77	4.70	66.91
	8	186.62	173.13	2.98	152.34
M	9	224.08	232.74	3.91	160.07
	10	153.76	163.09	2.67	138.45
	11	80.4	85.18	3.37	151.14
	13	363.99	308.28	5.18	147.53
	14	535.44	589.83	4.31	89.66
	16	163.13	262.15	18.06	28.33
H	17	224.08	181.36	9.44	28.94
	18	25.4	20.58	4.28	12.84
	19	110.05	108.35	11.34	23.98
	20	130.96	119.83	15.59	31.05

Table 3. Quantitative comparison of the team’s approach with ground truth using challenge dataset. The team evaluates their approach using Chamfer distance in $\times 10^{-3}$ with and without transformation metrics. Volumes in the table is in cm^3 .

MAPE ↓ (%)	Ch. w/ t.m ↓		Ch. w/o t.m ↓	
	sum	mean	sum	mean
10.973	0.130	0.007	1.715	0.095

Table 4. Quantitative comparison of the team’s approach with ground truth using challenge dataset. The team evaluates their approach using Chamfer distance with and without transformation metrics. The results show the mean and sum of the 18 scenes.

5. Second Place Team - ININ-VIAUN

5.1. Methodology

In this section, this team provides a detailed explanation of their proposed network, demonstrating how to progress from the original images to the final mesh models step by step. The code is available at <https://github.com/BIYia/cvpr-metafood>.

5.1.1 Scale factor estimation

The pipeline for coordinate-level scale factor estimation is shown in Figure 9. The team follows a corner projection matching method. Specifically, using the COLMAP[34] dense model, the team obtains the pose of each image as well as dense point cloud information. For any image img_k and its extrinsic parameters $[R/t]_k$, the team first performs a threshold-based corner detection with the threshold set to 240. This allows them to obtain the pixel coordinates of all detected corners. Subsequently, using the intrinsic parameters k and the extrinsic parameters $[R/t]_k$, the point cloud is

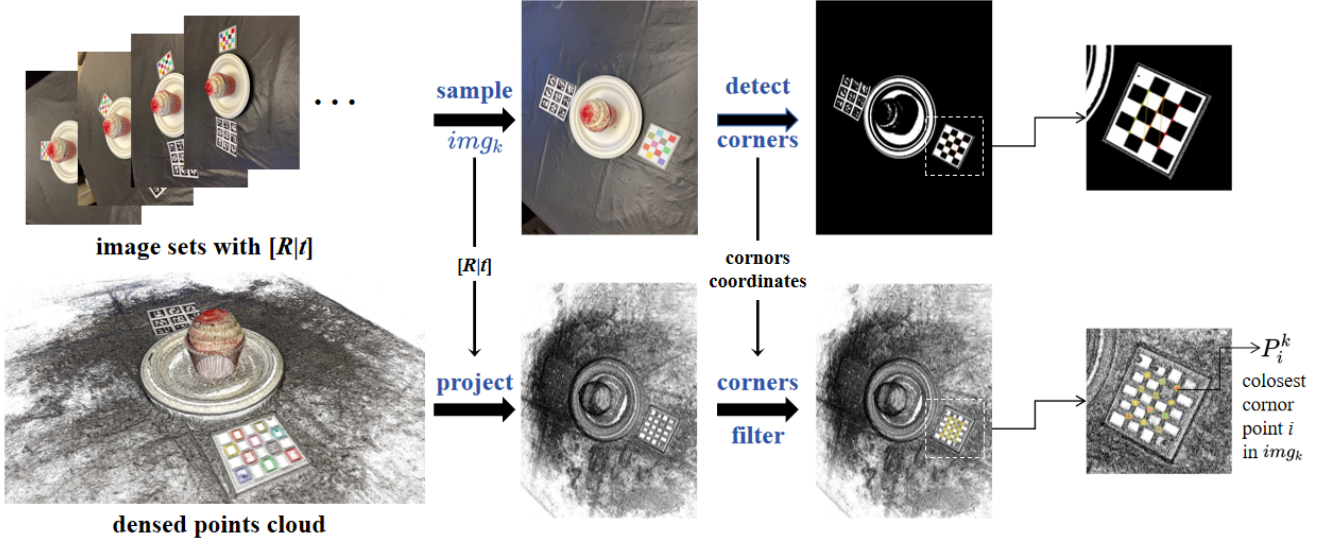


Figure 9. The pipeline of scale factor estimation.

projected onto the image plane. Based on the pixel coordinates of the corners, the team can identify the closest point coordinates P_i^k for each corner, where i represents the index of the corner. Thus, they can calculate the distance between any two corners as follows:

$$D_{ij}^k = \sqrt{(P_i^k - P_j^k)^2} \quad \forall i \neq j \quad (3)$$

To determine the final computed length of each checkerboard square in image k , the team takes the minimum value of each row of the matrix D^k (excluding the diagonal) to form the vector d^k . The median of this vector is then used. The final scale calculation formula is given by Equation 4, where 0.012 represents the known length of each square (1.2 cm):

$$\text{scale} = \frac{0.012}{\frac{1}{n} \sum_{i=1}^n \text{med}(d^k)} \quad (4)$$

5.1.2 3D Reconstruction

The pipeline for 3D reconstruction is shown in Figure 10. Considering the differences in input viewpoints, the team utilizes two pipelines to process the first fifteen objects and the last five single view objects.

For the first fifteen objects, the team uses COLMAP[34] to estimate the poses and segment the food using the provided segment masks in the dataset. Then, they apply advanced multi-view 3D reconstruction methods to reconstruct the segmented food. In practice, the team employs three different reconstruction methods: COLMAP[34], DiffusioNeRF[48], and NeRF2Mesh[41]. They select the best reconstruction results from these methods and extract

the mesh from the reconstructed model. Next, they scale the extracted mesh using the estimated scale factor. Finally, they apply some optimization techniques to obtain a refined mesh.

For the last five single-view objects, the team experiments with several single-view reconstruction methods, such as Zero123[21], Zero123++[38], One2345[20], ZeroNVS[31], and DreamGaussian[40]. They choose ZeroNVS[31] to obtain a 3D food model consistent with the distribution of the input image. In practice, they use the intrinsic camera parameters from the fifteenth object and employ an optimization method based on reprojection error to refine the extrinsic parameters of the single camera. However, due to the limitations of single-view reconstruction, the team needs to incorporate depth information from the dataset and the checkerboard in the monocular image to determine the size of the extracted mesh. Finally, they apply optimization techniques to obtain a refined mesh.

5.1.3 Mesh refinement

In the 3D Reconstruction phase, the team observes that the model’s results often suffer from low quality due to the presence of holes on the object surface and substantial noise, as illustrated in Figure 11.

To address the holes, the team employs MeshFix[1], an optimization method based on computational geometry. For surface noise, they utilize Laplacian Smoothing[2] for mesh smoothing operations. The Laplacian Smoothing method works by adjusting the position of each vertex to the average of its neighboring vertices:

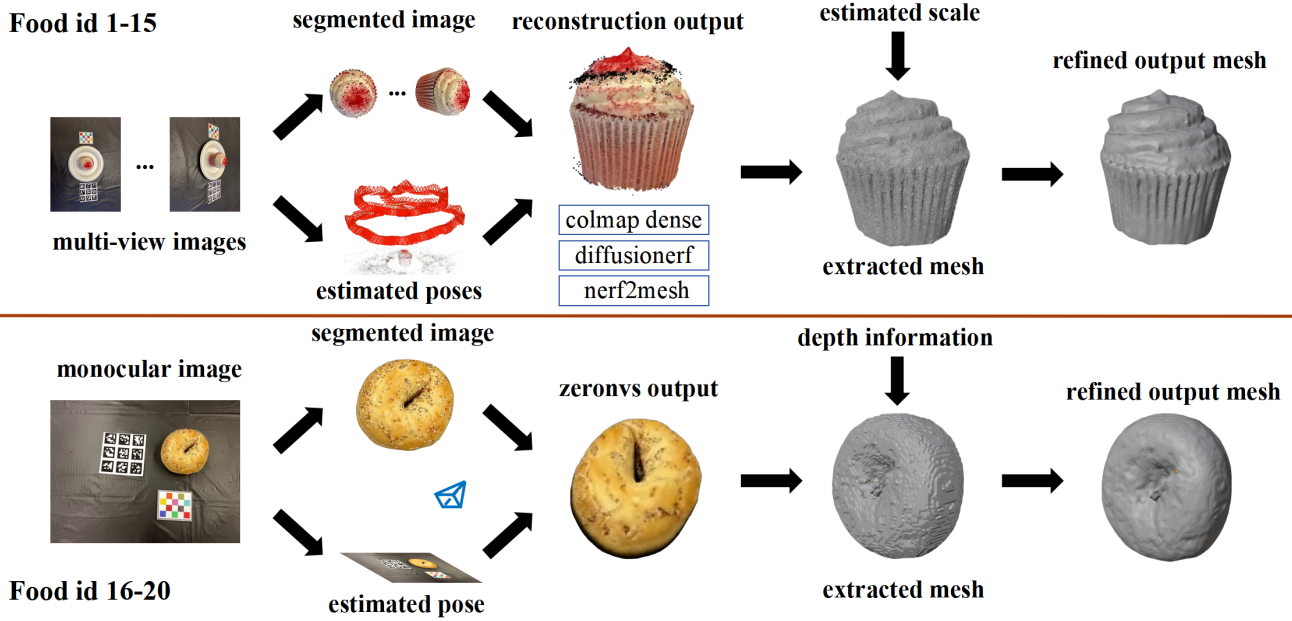


Figure 10. The pipeline of 3d reconstruction.

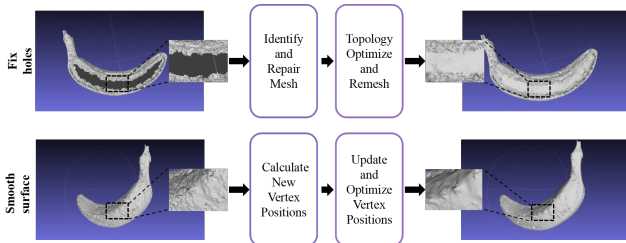


Figure 11. Mesh refinement.

$$v_i^{(new)} = v_i^{(old)} + \lambda \left(\frac{1}{N} \sum_{j \in \mathcal{N}(i)} v_j^{(old)} - v_i^{(old)} \right) \quad (3)$$

In their implementation, the team sets the smoothing factor λ to 0.2 and performs 10 iterations.

5.2. Experimental Results

5.2.1 Estimated scale factor

The scale factors estimated using the method described earlier are shown in Table 5. Each image and the corresponding reconstructed 3D model yield a scale factor, and the table presents the average scale factor for each object.

5.2.2 Reconstructed meshes

The refined meshes obtained using the methods described earlier are shown in Figure 12. The predicted model vol-

Object Index	Food Item	Scale Factor
1	Strawberry	0.060058
2	Cinnamon bun	0.081829
3	Pork rib	0.073861
4	Corn	0.083594
5	French toast	0.078632
6	Sandwich	0.088368
7	Burger	0.103124
8	Cake	0.068496
9	Blueberry muffin	0.059292
10	Banana	0.058236
11	Salmon	0.083821
13	Burrito	0.069663
14	Hotdog	0.073766

Table 5. Estimated scale factors.

umes, ground truth model volumes, and the percentage errors between them are shown in Table 6.

5.2.3 Alignment

The team designs a multi-stage alignment method for evaluating reconstruction quality. Figure 13 illustrates the alignment process for Object 14. First, the team calculates the central points of both the predicted model and the ground truth model, and moves the predicted model to align the central point of the ground truth model. Next, they perform ICP registration for further alignment, significantly reduc-

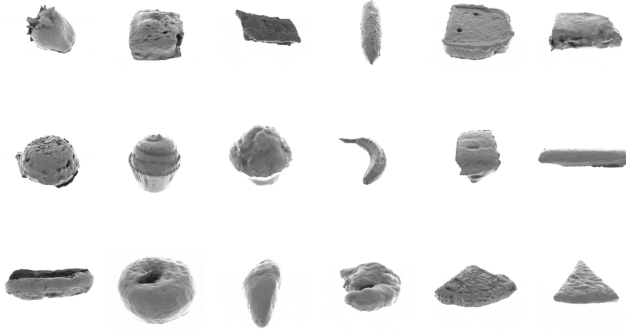


Figure 12. Refined Meshes.

Object Index	Predicted volume	Ground truth	Error percentage
1	44.51	38.53	15.52
2	321.26	280.36	14.59
3	336.11	249.67	34.62
4	347.54	295.13	17.76
5	389.28	392.58	0.84
6	197.82	218.44	9.44
7	412.52	368.77	11.86
8	181.21	173.13	4.67
9	233.79	232.74	0.45
10	160.06	163.09	1.86
11	86.0	85.18	0.96
13	334.7	308.28	8.57
14	517.75	589.83	12.22
16	176.24	262.15	32.77
17	180.68	181.36	0.37
18	13.58	20.58	34.01
19	117.72	108.35	8.64
20	117.43	119.83	20.03

Table 6. Metric of volume. The unit is cubic millimeters.

ing the Chamfer distance. Finally, they use gradient descent for additional fine-tuning, and obtain the final transformation matrix.

The total Chamfer distance between all 18 predicted models and the ground truths is 0.069441169.

6. Best 3D Mesh Reconstruction Team - FoodRiddle

6.1. Methodology

To achieve high-quality food mesh reconstruction, the team designed two pipeline processes as shown in Figure 14. For simple and medium cases, they employed a structure-from-motion approach to determine the pose of each image, followed by mesh reconstruction. Subsequently, a series of

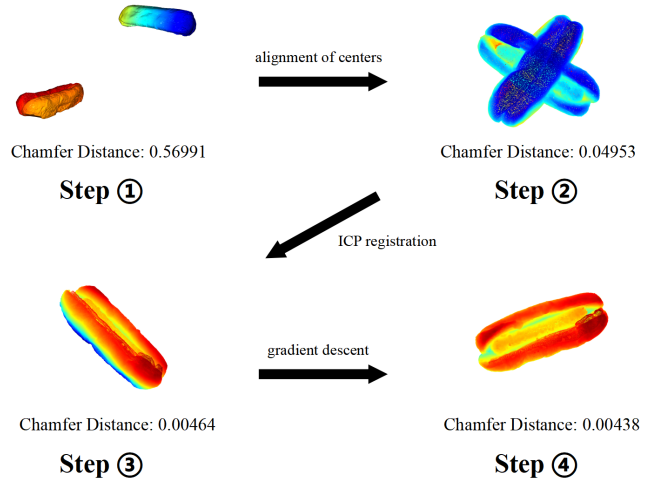


Figure 13. The process of aligning object 14.

post-processing steps were implemented to recalibrate scale and enhance mesh quality. For cases with only a single image, the team utilized image generation methods to aid in model generation.

6.1.1 Multi-View Reconstruction

For Structure from Motion (SfM), the team extended the state-of-the-art method COLMAP [33] by incorporating SuperPoint [6] and SuperGlue [32] methodologies. This significantly mitigated the issue of sparse keypoints in weakly textured scenes, as shown in Figure 15.

For mesh reconstruction, the team’s method is based on 2D Gaussian Splatting[13], which utilizes a differentiable 2D Gaussian renderer and incorporates regularization terms for depth distortion and normal consistency. The Truncated Signed Distance Function (TSDF) results are used to generate a dense point cloud.

In the post-processing stage, the team applied filtering and outlier removal techniques, identified the contour of the supporting surface, and projected the lower mesh vertices onto the supporting surface. They used the reconstructed checkerboard to rectify the scale of the model and used Poisson reconstruction to generate a watertight, complete mesh of the subject.

6.1.2 Single-View Reconstruction

For 3D reconstruction from a single image, the team employed state-of-the-art methods such as LGM[42], Instant Mesh[50], and One-2-3-45[19] to generate an initial prior mesh. This prior mesh was then jointly corrected with depth structure information.

To adjust the scale, the team estimated the object’s length using the checkerboard as a reference, assuming the object

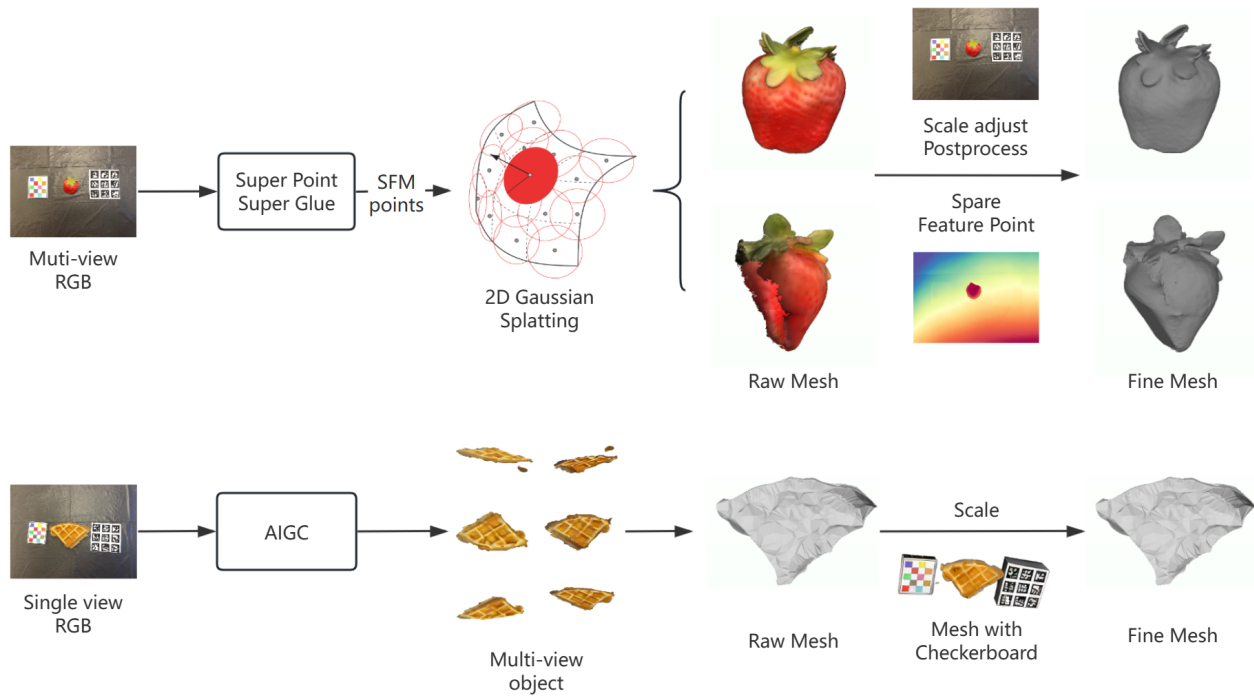


Figure 14. For multi-view image inputs, COLMAP integrated with SuperPoint and SuperGlue generates SFM points, which are used to create the initial Gaussian. Using 2D Gaussian Splatting, we obtain the mesh of the observed object. Subsequently, we adjust the mesh size and fit the unobserved underside of the object using the RGB checkerboard and depth maps. Finally, a complete and realistic food mesh is produced. For single-view input, we use the AIGC method to generate multi-view images consistent with the input image in 3D using a multi-view diffusion model. Then, using the Sparse-view Large Reconstruction Model, we directly predict the mesh. Lastly, using the simultaneously reconstructed checkerboard, adjust the size of the food.



Figure 15. The top left image showcases the vanilla COLMAP sfm points. The light-colored areas on the bread have fewer feature points, leading to the incomplete mesh in the top-right image. However, by integrating SuperPoint and SuperGlue into COLMAP, more interest points are obtained, resulting in an excellent final mesh, as shown in the bottom-right image.

and the checkerboard are on the same plane. They then projected the 3D object back onto the original 2D image to recover a more accurate scale of the object.

6.2. Experimental Results

Through a process of nonlinear optimization, the team sought to identify a transformation that minimizes the Chamfer distance between their mesh and the ground truth mesh. This optimization aimed to align the two meshes as closely as possible in three-dimensional space. Upon completion of this process, the average Chamfer distance across the final reconstructions of the 20 objects amounted to 0.0032175 meters. As shown in Table 7, Team FoodRiddle achieved the best scores for both multi-view and single-view reconstructions, outperforming other teams in the competition. The source code is available at <https://github.com/jlyw1017/FoodRiddle-MetaFood-CVPR2024>.

7. Conclusion

In this report, we review and summarize the methods and results of the MetaFood CVPR Workshop challenge on 3D

Team	Multi-view (1-14)	Single-view (16-20)
FoodRiddle	0.036362	0.019232
ININ-VIAUN	0.041552	0.027889
VoIETA	0.071921	0.058726

Table 7. Total Errors for Different Teams on Multi-view and Single-view Data. Team FoodRiddle has the best score.

Food Reconstruction. The challenge aimed to advance 3D reconstruction techniques by focusing on food items, addressing the unique challenges posed by varying textures, reflective surfaces, and complex geometries typical in culinary subjects.

The competition utilized 20 diverse food items, captured under different conditions and with varying numbers of input images, specifically designed to challenge participants in developing robust reconstruction models. The evaluation was based on a two-phase process, assessing both portion size accuracy through Mean Absolute Percentage Error (MAPE) and shape accuracy using the Chamfer distance metric.

Out of all participating teams, three made it to the final submission, showcasing a range of innovative solutions. Team VoIETA won the first place with the overall best performance on both Phase-I and Phase-II. Followed by team ININ-VIAUN who won the second place. In addition, FoodRiddle team demonstrated superior performance in Phase-II, indicating a competitive and high-caliber field of entries for 3D mesh reconstruction. The challenge has successfully pushed the boundaries of 3D food reconstruction, demonstrating the potential for accurate volume estimation and shape reconstruction in nutritional analysis and food presentation applications. The innovative approaches developed by the participating teams provide a solid foundation for future research in this field, potentially leading to more accurate and user-friendly methods for dietary assessment and monitoring.

References

- [1] Marco Attene. A lightweight approach to repairing digitized polygon meshes. *The Visual Computer*, 2010. 9
- [2] Another Author. Locality-aware laplacian mesh smoothing. *arXiv preprint arXiv:1606.00803*, 2016. 9
- [3] Maksym Bekuzarov, Ariana Bermudez, Joon-Young Lee, and Hao Li. Xmem++: Production-level video segmentation from few annotated frames. In *Proceedings of the IEEE/CVF International Conference on Computer Vision*, pages 635–644, 2023. 4
- [4] Paolo Cignoni, Marco Callieri, Massimiliano Corsini, Matteo Dellepiane, Fabio Ganovelli, Guido Ranzuglia, et al. Meshlab: an open-source mesh processing tool. In *Eurographics Italian chapter conference*, pages 129–136. Salerno, Italy, 2008. 5
- [5] Kanjar De and V Masilamani. Image sharpness measure for blurred images in frequency domain. *Procedia Engineering*, 64:149–158, 2013. 4
- [6] Daniel DeTone, Tomasz Malisiewicz, and Andrew Rabinovich. Superpoint: Self-supervised interest point detection and description. In *2018 IEEE/CVF Conference on Computer Vision and Pattern Recognition Workshops (CVPRW)*, pages 337–33712, 2018. 11
- [7] Daniel DeTone, Tomasz Malisiewicz, and Andrew Rabinovich. Superpoint: Self-supervised interest point detection and description. In *Proceedings of the IEEE conference on computer vision and pattern recognition workshops*, pages 224–236, 2018. 4
- [8] Anqi Gao, Frank P.-W. Lo, and Benny Lo. Food volume estimation for quantifying dietary intake with a wearable camera. *Proceedings of the 2018 IEEE 15th International Conference on Wearable and Implantable Body Sensor Networks*, pages 110–113, 2018. 2
- [9] Jiangpeng He and Fengqing Zhu. Online continual learning for visual food classification. *Proceedings of the IEEE/CVF International Conference on Computer Vision Workshops*, pages 2337–2346, 2021. 2
- [10] Jiangpeng He, Zeman Shao, Janine Wright, Deborah Kerr, Carol Boushey, and Fengqing Zhu. Multi-task image-based dietary assessment for food recognition and portion size estimation. *2020 IEEE Conference on Multimedia Information Processing and Retrieval*, pages 49–54, 2020. 2
- [11] Jiangpeng He, Runyu Mao, Zeman Shao, Janine L Wright, Deborah A Kerr, Carol J Boushey, and Fengqing Zhu. An end-to-end food image analysis system. *Electronic Imaging*, 2021(8):285–1, 2021. 2
- [12] Jiangpeng He, Luotao Lin, Heather A Eicher-Miller, and Fengqing Zhu. Long-tailed food classification. *Nutrients*, 15(12):2751, 2023. 2
- [13] Binbin Huang, Zehao Yu, Anpei Chen, Andreas Geiger, and Shenghua Gao. 2d gaussian splatting for geometrically accurate radiance fields. *arXiv preprint arXiv:2403.17888*, 2024. 11
- [14] Yuning Huang, M A Hassan, Jiangpeng He, Janine Higgins, Megan McCrory, Heather Eicher-Miller, J Graham Thomas, Edward Sazonov, and Fengqing Zhu. Automatic recognition of food ingestion environment from the aim-2 wearable sensor. *Proceedings of the IEEE/CVF Conference on Computer Vision and Pattern Recognition*, pages 3685–3694, 2024. 2
- [15] Tanuj Jain, Christopher Lennan, Zubin John, and Dat Tran. Imagededup. <https://github.com/ideal0/imagededup>, 2019. 4
- [16] Wenyan Jia, Yaofeng Yue, John D Fernstrom, Zhengnan Zhang, Yongquan Yang, and Mingui Sun. 3d localization of circular feature in 2d image and application to food volume estimation. *Proceedings of the 2012 Annual International Conference of the IEEE Engineering in Medicine and Biology Society*, pages 4545–4548, 2012. 2
- [17] Alexander Kirillov, Eric Mintun, Nikhila Ravi, Hanzi Mao, Chloe Rolland, Laura Gustafson, Tete Xiao, Spencer Whitehead, Alexander C Berg, Wan-Yen Lo, et al. Segment anything. In *Proceedings of the IEEE/CVF International Conference on Computer Vision*, pages 4015–4026, 2023. 4

- [18] Philipp Lindenberger, Paul-Edouard Sarlin, Viktor Larsson, and Marc Pollefeys. Pixel-perfect structure-from-motion with featuremetric refinement. In *Proceedings of the IEEE/CVF international conference on computer vision*, pages 5987–5997, 2021. 4, 6
- [19] Minghua Liu, Chao Xu, Haian Jin, Linghao Chen, Mukund Varma T, Zexiang Xu, and Hao Su. One-2-3-45: Any single image to 3d mesh in 45 seconds without per-shape optimization. *Advances in Neural Information Processing Systems*, 36, 2024. 11
- [20] Minghua Liu, Chao Xu, Haian Jin, Linghao Chen, Mukund Varma T, Zexiang Xu, and Hao Su. One-2-3-45: Any single image to 3d mesh in 45 seconds without per-shape optimization. *Advances in Neural Information Processing Systems*, 36, 2024. 6, 8, 9
- [21] Ruoshi Liu, Rundi Wu, Basile Van Hoorick, Pavel Tokmakov, Sergey Zakharov, and Carl Vondrick. Zero-1-to-3: Zero-shot one image to 3d object. In *Proceedings of the IEEE/CVF International Conference on Computer Vision*, pages 9298–9309, 2023. 8, 9
- [22] Frank P.-W. Lo, Yingnan Sun, and Benny Lo. Depth estimation based on a single close-up image with volumetric annotations in the wild: A pilot study. *Proceedings of the 2019 IEEE/ASME International Conference on Advanced Intelligent Mechatronics*, pages 513–518, 2019. 3
- [23] Frank Po Wen Lo, Yingnan Sun, Jianing Qiu, and Benny Lo. Image-Based Food Classification and Volume Estimation for Dietary Assessment: A Review. *IEEE Journal of Biomedical and Health Informatics*, 24(7):1926–1939, 2020. 2
- [24] Runyu Mao, Jiangpeng He, Luotao Lin, Zeman Shao, Heather A. Eicher-Miller, and Fengqing Zhu. Improving dietary assessment via integrated hierarchy food classification. *2021 IEEE 23rd International Workshop on Multimedia Signal Processing (MMSP)*, pages 1–6, 2021. 2
- [25] Runyu Mao, Jiangpeng He, Zeman Shao, Sri Kalyan Yarlagadda, and Fengqing Zhu. Visual aware hierarchy based food recognition. *Proceedings of the International conference on pattern recognition*, pages 571–598, 2021.
- [26] Weiqing Min, Zhiling Wang, Yuxin Liu, Mengjiang Luo, Liping Kang, Xiaoming Wei, Xiaolin Wei, and Shuqiang Jiang. Large scale visual food recognition. *IEEE Transactions on Pattern Analysis and Machine Intelligence*, 45(8): 9932–9949, 2023.
- [27] Xinyue Pan, Jiangpeng He, and Fengqing Zhu. Personalized food image classification: Benchmark datasets and new baseline. In *2023 57th Asilomar Conference on Signals, Systems, and Computers*, pages 1095–1099. IEEE, 2023. 2
- [28] Manika Puri, Zhiwei Zhu, Qian Yu, Ajay Divakaran, and Harpreet Sawhney. Recognition and volume estimation of food intake using a mobile device. *Proceedings of the 2009 Workshop on Applications of Computer Vision*, pages 1–8, 2009. 2
- [29] Md Hafizur Rahman, Qiang Li, Mark Pickering, Michael Frater, Deborah Kerr, Carol Bouche, and Edward Delp. Food volume estimation in a mobile phone based dietary assessment system. *Proceedings of the 2012 8th International Conference on Signal Image Technology and Internet Based Systems*, pages 988–995, 2012. 2
- [30] Szymon Rusinkiewicz and Marc Levoy. Efficient variants of the icp algorithm. In *Proceedings third international conference on 3-D digital imaging and modeling*, pages 145–152. IEEE, 2001. 6
- [31] Kyle Sargent, Zizhang Li, Tanmay Shah, Charles Herrmann, Hong-Xing Yu, Yunzhi Zhang, Eric Ryan Chan, Dmitry Lagun, Li Fei-Fei, Deqing Sun, et al. Zernovs: Zero-shot 360-degree view synthesis from a single image. In *Proceedings of the IEEE/CVF Conference on Computer Vision and Pattern Recognition*, pages 9420–9429, 2024. 9
- [32] Paul-Edouard Sarlin, Daniel DeTone, Tomasz Malisiewicz, and Andrew Rabinovich. Superglue: Learning feature matching with graph neural networks. In *Proceedings of the IEEE/CVF conference on computer vision and pattern recognition*, pages 4938–4947, 2020. 4, 11
- [33] Johannes Lutz Schönberger and Jan-Michael Frahm. Structure-from-motion revisited. In *Conference on Computer Vision and Pattern Recognition (CVPR)*, 2016. 11
- [34] Johannes L Schonberger and Jan-Michael Frahm. Structure-from-motion revisited. In *Proceedings of the IEEE conference on computer vision and pattern recognition*, pages 4104–4113, 2016. 8, 9
- [35] Zeman Shao, Shaobo Fang, Runyu Mao, Jiangpeng He, Janine L. Wright, Deborah A. Kerr, Carol J. Boushey, and Fengqing Zhu. Towards learning food portion from monocular images with cross-domain feature adaptation. *Proceedings of 2021 IEEE 23rd International Workshop on Multimedia Signal Processing*, pages 1–6, 2021. 2, 3
- [36] Zeman Shao, Yue Han, Jiangpeng He, Runyu Mao, Janine Wright, Deborah Kerr, Carol Jo Boushey, and Fengqing Zhu. An integrated system for mobile image-based dietary assessment. *Proceedings of the 3rd Workshop on AIXFood*, page 19–23, 2021. 2
- [37] Zeman Shao, Gautham Vinod, Jiangpeng He, and Fengqing Zhu. An end-to-end food portion estimation framework based on shape reconstruction from monocular image. *Proceedings of 2023 IEEE International Conference on Multimedia and Expo*, pages 942–947, 2023. 3
- [38] Ruoxi Shi, Hansheng Chen, Zhuoyang Zhang, Minghua Liu, Chao Xu, Xinyue Wei, Linghao Chen, Chong Zeng, and Hao Su. Zero123++: a single image to consistent multi-view diffusion base model. *arXiv preprint arXiv:2310.15110*, 2023. 9
- [39] Jan Steinbrener, Vesna Dimitrievska, Federico Pittino, Frans Starmans, Roland Waldner, Jürgen Holzbauer, and Thomas Arnold. Learning metric volume estimation of fruits and vegetables from short monocular video sequences. *Heliyon*, 9(4), 2023. 8
- [40] Jiaxiang Tang, Jiawei Ren, Hang Zhou, Ziwei Liu, and Gang Zeng. Dreamgaussian: Generative gaussian splatting for efficient 3d content creation. *arXiv preprint arXiv:2309.16653*, 2023. 9
- [41] Jiaxiang Tang, Hang Zhou, Xiaokang Chen, Tianshu Hu, Errui Ding, Jingdong Wang, and Gang Zeng. Delicate textured mesh recovery from nerf via adaptive surface refinement. In *Proceedings of the IEEE/CVF International Conference on Computer Vision*, pages 17739–17749, 2023. 9

- [42] Jiaxiang Tang, Zhaoxi Chen, Xiaokang Chen, Tengfei Wang, Gang Zeng, and Ziwei Liu. Lgm: Large multi-view gaussian model for high-resolution 3d content creation. *arXiv preprint arXiv:2402.05054*, 2024. [11](#)
- [43] Quin Thames, Arjun Karapur, Wade Norris, Fangting Xia, Liviu Panait, Tobias Weyand, and Jack Sim. Nutrition5k: Towards automatic nutritional understanding of generic food. In *Proceedings of the IEEE/CVF conference on computer vision and pattern recognition*, pages 8903–8911, 2021. [3](#), [7](#)
- [44] Frances E Thompson and Amy F Subar. Dietary assessment methodology. *Nutrition in the Prevention and Treatment of Disease*, pages 5–48, 2017. [2](#)
- [45] Gautham Vinod, Zeman Shao, and Fengqing Zhu. Image based food energy estimation with depth domain adaptation. *Proceedings of 2022 IEEE 5th International Conference on Multimedia Information Processing and Retrieval*, pages 262–267, 2022. [3](#)
- [46] Gautham Vinod, Jiangpeng He, Zeman Shao, and Fengqing Zhu. Food portion estimation via 3d object scaling. *Proceedings of the IEEE/CVF Conference on Computer Vision and Pattern Recognition*, pages 3741–3749, 2024. [2](#)
- [47] Yiming Wang, Qin Han, Marc Habermann, Kostas Daniilidis, Christian Theobalt, and Lingjie Liu. Neus2: Fast learning of neural implicit surfaces for multi-view reconstruction. In *Proceedings of the IEEE/CVF International Conference on Computer Vision*, pages 3295–3306, 2023. [4](#)
- [48] Jamie Wynn and Daniyar Turmukhambetov. Diffusionerf: Regularizing neural radiance fields with denoising diffusion models. In *Proceedings of the IEEE/CVF Conference on Computer Vision and Pattern Recognition*, pages 4180–4189, 2023. [9](#)
- [49] Chang Xu, Ye He, Nitin Khanna, Carol J. Boushey, and Edward J. Delp. Model-based food volume estimation using 3d pose. *Proceedings of the 2013 IEEE International Conference on Image Processing*, pages 2534–2538, 2013. [2](#)
- [50] Jiale Xu, Weihao Cheng, Yiming Gao, Xintao Wang, Shenghua Gao, and Ying Shan. Instantmesh: Efficient 3d mesh generation from a single image with sparse-view large reconstruction models. *arXiv preprint arXiv:2404.07191*, 2024. [11](#)